Electronic Supplementary Information

HF-resistant Perfluorinated Porous Polymer for Separation of Electronic Specialty Gases

Weiwei Zhang,‡[a] Hui Yin,‡[a] Jiawu Huang,[a] Xiaoying Zhou,[a] Cuiting Yang,[a] Zilu Zhang,[a] Junjie Peng*[a,b] and Jing Xiao*[a]

[a] Guangdong Provincial Key Laboratory of Green Chemical Product Technology, School of Chemistry and Chemical Engineering, South China University of Technology, Guangzhou, 510641, P.R. China. Email: cejingxiao@scut.edu.cn
[b] School of Environment and Chemical Engineering, Foshan University, Foshan 528000, PR China. Email: cepengjunjie@fosu.edu.cn

‡ W.Z and H.Y. contributes equally to this work.

Materials

All reagents were commercially available and used as received without further purification. Perfluorobenzene (PFB, 392-56-3), octafluoronaphthalene (OFN, 313-72-4), (trimethylsilyl)acetylene (TMSA, 1066-54-2), 1,2-bis(trimethylsilyl)acetylene (BTMSA, 14630-40-1), and 1 M solution of tetrabutylammonium fluoride (TBAF, 429-41-4) were purchased from Energy Chemical (Anhui Senrise Technology Co., Ltd.). The solvents were extra-dry, such as N,N-dimethylformamide (DMF, 68-12-2), tetrahydrofuran (THF, 109-99-9) and toluene (108-88-3). All the gases, e.g. nitrogen trifluoride (NF_3), carbon tetrafluoride (CF_4), and sulfur hexafluoride (SF_6) were purchased from Guangdong Huate Gas Co., Ltd. The zeolites, including 5A and HZSM-5 (H-type ZSM-5), used in the tests were purchased from The Catalyst Plant of Nankai University, while the metal-organic framework, ZIF-67, was synthesized according to previous reports.

Methods

Synthesis of PFPPs:

The synthesis of PFPPs was carried out via a nucleophilic aromatic substitution (S_NAr) reaction. Under an inert atmosphere and controlled temperature, perfluoroarene (monomer **A**, 10 mmol) and the corresponding proportion of monomer **B** (silylacetylene) were dissolved in an extra-dry solvent. While stirring, the appropriate amount of catalyst at the specified concentration was added dropwise at a rate of one drop every 3 seconds using a needle. The initially colorless, transparent solution gradually darkened, viscosity increased, and gas was released. The mixture was then stirred overnight at controlled temperatures. Considering the yield, specific surface area (S_{BET}), and cost, the product synthesized under the optimal conditions is referred to as PFPP-1.

The proposed mechanism for PFPP-1 formation was illustrated in Fig. S1. Under basic F^- catalysis, monomer **B** undergoes desilylation, generating an activated acetylide anion. This anion subsequently nucleophilically attacks the perfluoroarene (monomer **A**), forming stable C-C bonds and releasing trimethylsilyl fluoride (TMSF) gas. This process drives the polymerization, resulting in a cross-linked polymer network. Building on the foundation of Yavuz's group[1] (COP-177), this study focuses on optimizing the synthesis conditions for the polymer. Both monomer **B** and the catalyst in this reaction are highly sensitive to moisture and oxygen, with the anhydrous and anaerobic conditions significantly influencing the material's specific surface area, pore structure, and yield. These limitations pose challenges to the scalability and practicality of the polymer, which this study aims to address. We simplified the synthesis procedure (Fig. S2-4) to enhance the scalability of PFPP-1. Compared to the previous method, the need for complex solvent degassing steps was eliminated, and increasing the amount of an inexpensive non-metal catalyst (TBAF) efficiently improved the yield, overcoming the effects of dissolved O_2 and moisture (Fig. S2) in the reaction system.

The effect of the following synthesis variables was systematically investigated to optimize the polymerization conditions.

(i) Monomer Types. Two types of monomer **A**, including perfluorobenzene (PFB) and octafluoronaphthalene (OFN), and monomer **B**, including (trimethylsilyl)acetylene (TMSA) and 1,2-bis(trimethylsilyl)acetylene (BTMSA), were evaluated for the synthesis. PFB, as a more electron-deficient electrophile reagent than OFN, exhibits higher S_NAr reactivity. For monomer B, although theoretically BTMSA should exhibit higher reactivity than TMSA—due to the greater affinity of the TMS group for F^- compared to the terminal alkyne's H atom, which should promote a faster reaction rate in the second activation step (Fig. S1)—experimental results suggest the opposite. This discrepancy is likely due to the

larger steric hindrance of the TMS group[2]. Hence, the combination of PFB and TMSA, which exhibited the fastest polymerization rate, was selected as the optimal monomers.

(ii) **B**/**A** ratio. Different monomer ratios (**B**/**A** = 1, 2, 3) were investigated for synthesis. Among these, the **B**/**A** ratio of 2 was found to be the most economical choice, considering both S_{BET} and yield.

(iii) Temperature. To elucidate the role of the release of TMSF in determining the S_{BET} of the polymer, different reaction temperatures (T = 10, 25, 35°C) were investigated. At 10°C, which is below the boiling point of TMSF (~16.4°C), the yield remained almost unchanged, but the S_{BET} significantly decreased. This reduction was attributed to TMSF remaining dissolved in the solvent, causing the polymer chains to form efficient "parallel and tight" packing, leading to low porosity. When the temperature exceeded 25°C, neither yield nor S_{BET} showed significant improvement. Therefore, 25°C was selected as the most cost-effective temperature.

(iv) Catalyst droplet concentration. The S_{BET} increased with higher droplet concentration (c = 0.1, 0.5, 1.0 M), while the yield was inversely proportional to it. A higher catalyst concentration promotes a rapid initial reaction rate, favoring fast nucleation and rapid release of TMSF, which is beneficial for building high-porosity polymers. However, it also leads to the entrapment of highly polar TBAF[3] in the polymer pores, resulting in incomplete subsequent reactions. In contrast, using a lower catalyst concentration requires more droplets and provides better dispersion in the increasingly viscous system, leading to higher-yield but lower-porosity polymers.

Characterization:

N_2 adsorption-desorption isotherms at 77 K were obtained using a Micromeritics 3-Flex surface characterization analyzer. Adsorption isotherms of N_2, NF_3, CF_4, and SF_6 at 298 K were measured in a similar manner. For each test, the total surface area of the sample was no less than 40 m^2, and all materials were degassed under vacuum at 373 K for over 3 hours prior to testing to remove the adsorbed CO_2 and H_2O. The pore volume and pore size distribution were analyzed using the Non-Local Density Functional Theory (NLDFT) model, while the specific surface area (S_{BET}) was calculated from the adsorption isotherms based on the Brunauer-Emmett-Teller model. The morphology of the samples was observed by scanning electron microscopy (SEM, Hitachi SU8220) at 5.0 kV acceleration voltage. The functional groups were characterized via Fourier-transform infrared spectroscopy (FTIR) in the range of 500-4000 cm^{-1} (Nicolet IS50-Nicolet Continuum). The surface chemical states were examined by X-ray photoelectron spectroscopy (XPS, Thermo Scientific K-Alpha) equipped with Al Kα as an exciting X-ray source. Calibration must be carefully performed by uniformly mixing fine PTFE powder into COP-177 and adjusting the C-F_2 peak in the C1s spectrum (attributed to PTFE) to 292.5 eV[4], which resulted in a binding energy of 288.2 eV for the covalent C-F characteristic peak. The chemical composition (C, H, N, and O) of the samples was determined using an elemental analyzer (EA, Elementar Vario EL). Fluorine content was directly calculated from EA results and corroborated by combustion ion chromatography (CIC), with elemental composition further confirmed by XPS and Energy-Dispersive X-ray Spectroscopy (EDX).

IAST selectivity:

The adsorption isotherms of N_2, NF_3, CF_4 and SF_6 at 298 K were first fitted using the Langmuir-Freundlich model, followed by calculating the adsorption selectivity for binary F-gas/N_2 mixtures using IAST (F-gas/N_2 = 1/9). The expression for the Langmuir-Freundlich model is depicted as follows:

$$q = \frac{Nap^b}{1 + ap^b}$$

where q is the adsorbed amount (mmol/g), N is the maximum adsorption capacity (mmol/g), a is the affinity constant (1/kPa), p is the pressure (kPa), and b is the heterogeneity factor.
The expression for IAST selectivity is depicted as follows:

$$S = \frac{q_A/y_A}{q_B/y_B}$$

where S represents the selectivity of component A over component B; q_A and q_B are the adsorbed amounts of components A and B, respectively, and y_A and y_B are their respective mole fractions in the gas phase.
Breakthrough experiments:
The dynamic breakthrough experiment was carried out on a fixed-bed. Conditions of the feed stream were designed to equimolar composition of gas mixture (F-gases/N_2 = 2/98 volume ratio) at 298 K and 1 bar. For the breakthrough test, the following parameter values were used: the weight of adsorbent, 400 mg; the flow rate the mixture,10 mL/min. The flow rate of the gas mixture was controlled using mass flow meters. The outlet gas from the column was monitored with a gas chromatography-thermal conductivity detector (GC-TCD), with hydrogen as the carrier gas. The analysis of each fraction of the sample was completed within 1.2 min. The composition of the outlet gas was continuously recorded. The adsorption capacity (Q) of the adsorbent for a gas can be calculated using the following equation,

$$Q_i = \frac{V_T P_i \Delta t}{m}$$

Here, V_T (mL/min) is the total gas flow; P_i is the partial pressure of this gas in the gas mixture; Δt (min) is the breakthrough time; m (g) is the mass of adsorbent.
The dynamic selectivity of breakthrough experiments can be measured by separation factors (S),

$$S = \frac{Q_1 y_2}{Q_2 y_1}$$

Calculation of heat of adsorption:
The heat of adsorption (Q_{st}) can be calculated by fitting the adsorption isotherms at varied temperatures using the Virial equation:

$$\ln(P) = \ln N + 1/T \sum_{i=0}^{m} a_i N_i + \sum_{j=0}^{n} b_j N_j$$

where P is the adsorption pressure (bar), N is the uptake (mmol g^{-1}), T is the temperature (K), m and n represent the number of coefficients required to adequately describe the isotherms, and a_i and b_j refer to the Virial coefficients. The values of Virial coefficients a_0–a_m can then be used to calculate the heat of absorption using the following expression:

$$Q_{st} = -R \sum_{i=0}^{m} a_i N_i$$

where Q_{st} is the coverage-dependent heat of adsorption and R refers to the ideal gas constant. In this study, the Q_{st} of F-gases was determined using the data from the isotherms at 273, 288, and 298 K in the pressure range of 0-1 bar.
DFT Simulations:
Selected gas molecules' binding energy and electrostatic potential (e.g., N_2, NF_3, CF_4, SF_6, HF) with polymer fragments were carried out with the Gaussian 16 software. The B3LYP functional[5] was adopted for all calculations in combination with the D3BJ dispersion correction[6]. Geometry optimization and

frequency calculations were at the level of 6-31G(d,p) for all atoms[7, 8].The single point calculations were at the level of M062x-D3/6-311G(d, p)[9, 10].

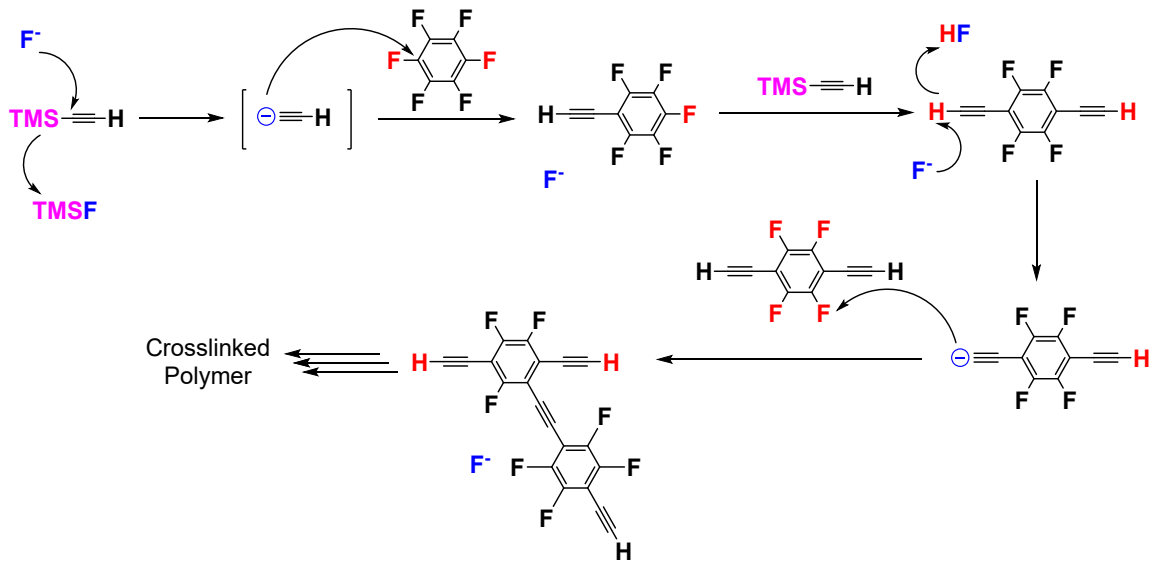

Fig. S1 Proposed mechanism for PFPP-1 formation[1]. Theoretically, this reaction requires a basic "naked" F^- catalyst, However, the presence of moisture in the system can bind with F^-, leading to the loss of its catalytic activity. Similarly, the deprotonation of alkynes can also result in F^- deactivation. Therefore, increasing the amount of an inexpensive non-metal catalyst, TBAF, can efficiently counteract the dissolved moisture in the reaction system.

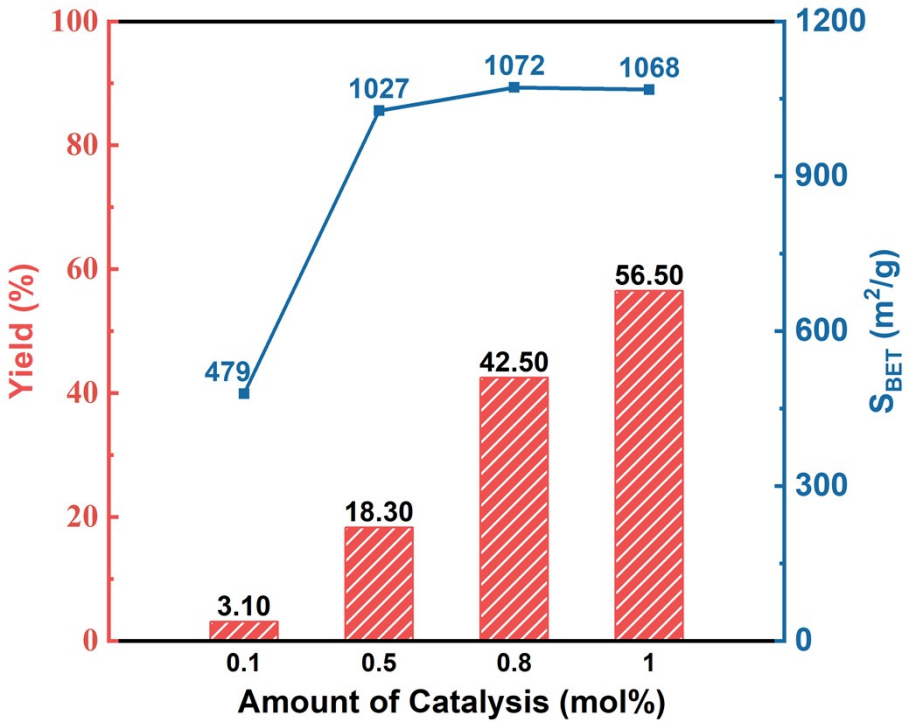

Fig. S2 Optimization of catalyst amount in PFPP-1 synthesis. Increasing the amount of an inexpensive non-metal catalyst (TBAF) efficiently improved the yield, overcoming the effects of dissolved O_2 and moisture in the reaction system. The need for complex solvent degassing steps by liquid N_2 for 3 times was eliminated.

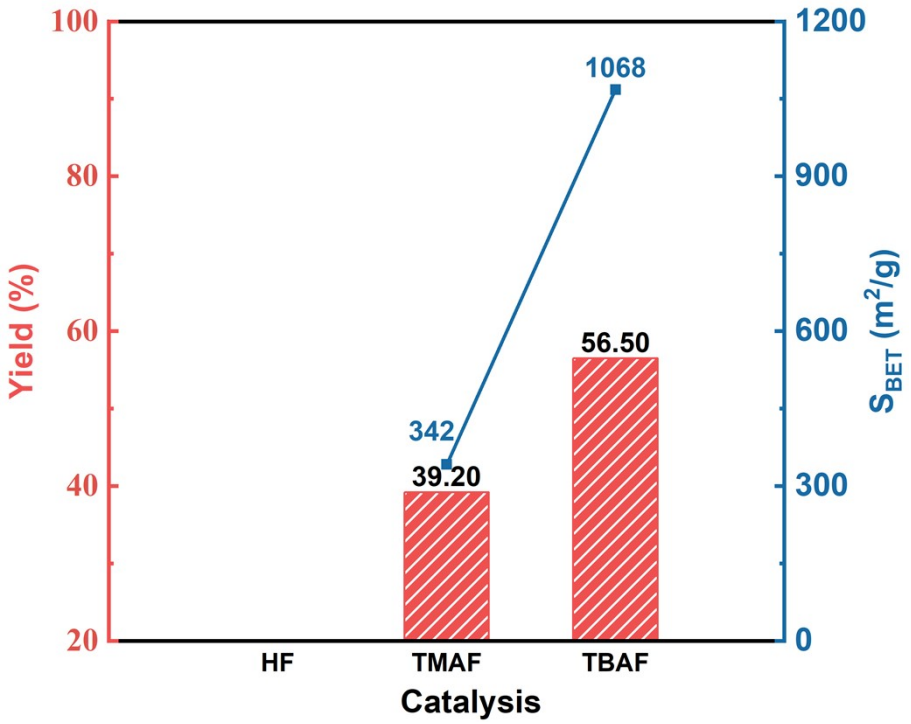

Fig. S3 Optimization of catalyst type in PFPP-1 synthesis. TBAF exhibits the best catalytic performance, followed by TMAF, while HF shows no catalytic ability, indicating that only basic "naked" F^- possesses catalytic activity. Basic F^- sources, such as TMAF, TBAF, or metallic F^- sources[11], exhibit catalytic properties. Although TMAF is more anhydrous[12] than TBAF[13, 14], its lower catalytic performance can be attributed to its poor solubility (TMAF cannot form a 1 M solution in either DMF or THF).

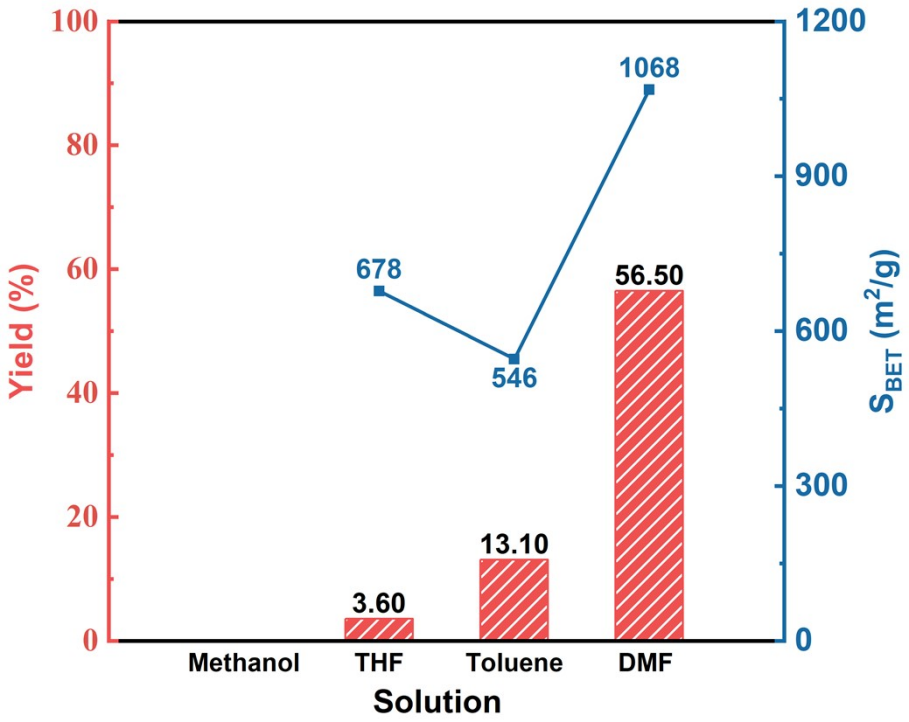

Fig. S4 Optimization of solvent type in PFPP-1 synthesis. The product cannot be obtained in MeOH because the protic solvent coordinates with F^-, leading to catalyst deactivation. Thus, the reaction must be carried out in an aprotic solvent. Among aprotic solvents, polar DMF demonstrates the best performance, likely due to its superior solubility for both substrates and oligomers. This delays phase separation, facilitating the formation of polymers with a higher degree of polymerization, abundant microporosity, and a larger specific surface area[15, 16].

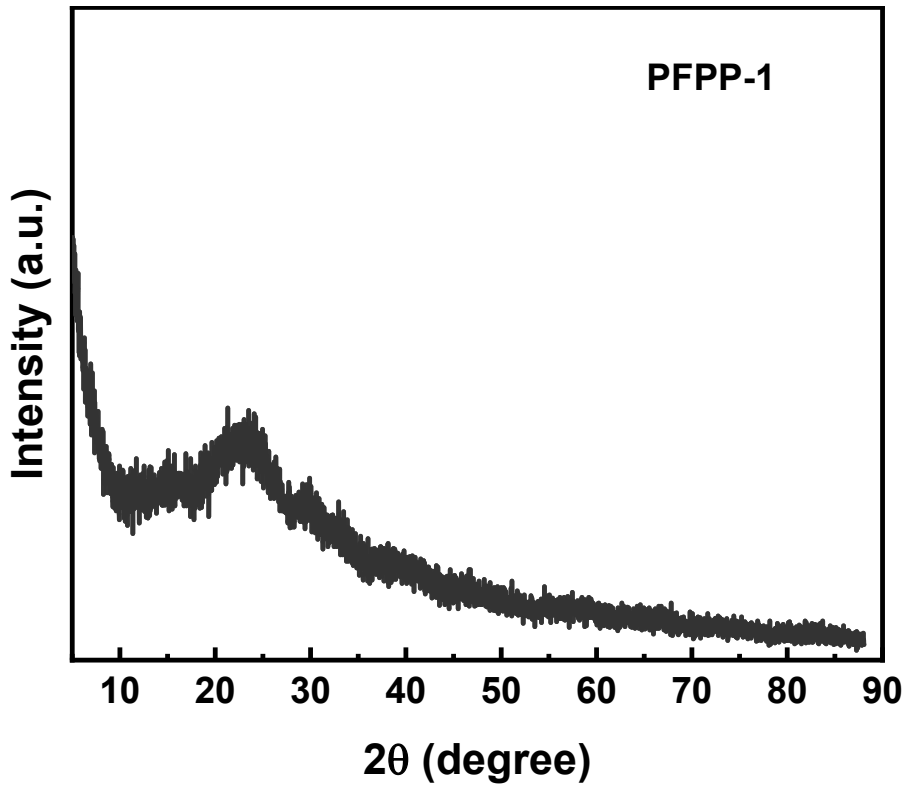

Fig. S5 Powder X-ray diffraction (PXRD) pattern of amorphous PFPP-1.

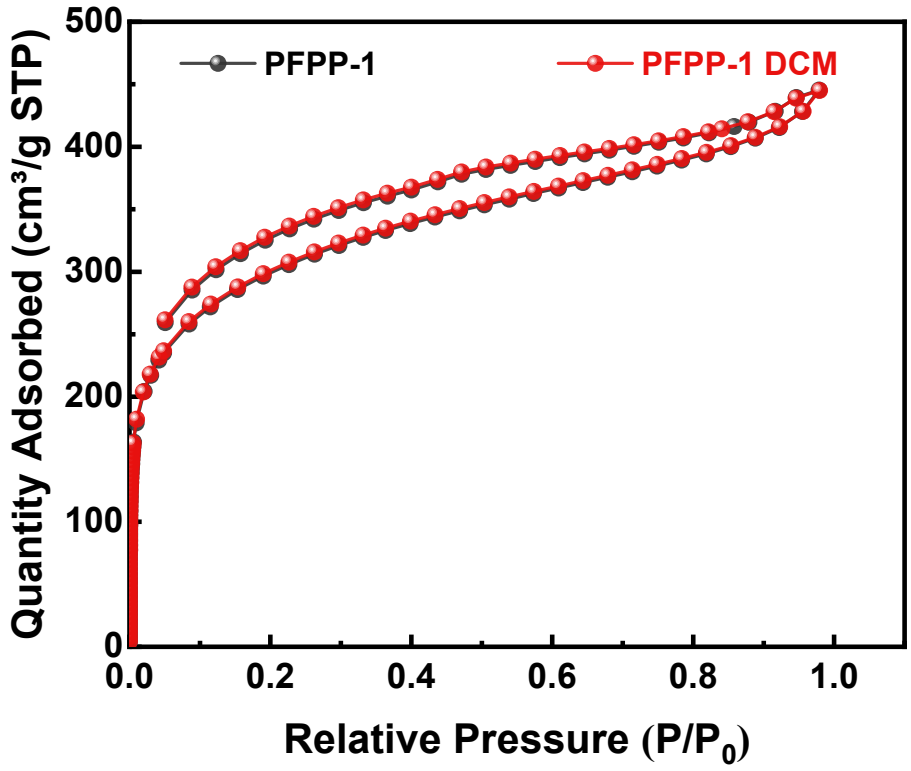

Fig. S6 N_2 adsorption-desorption isotherms at 77 K of pristine PFPP-1 and PFPP-1 immersed in DCM for 24 hours

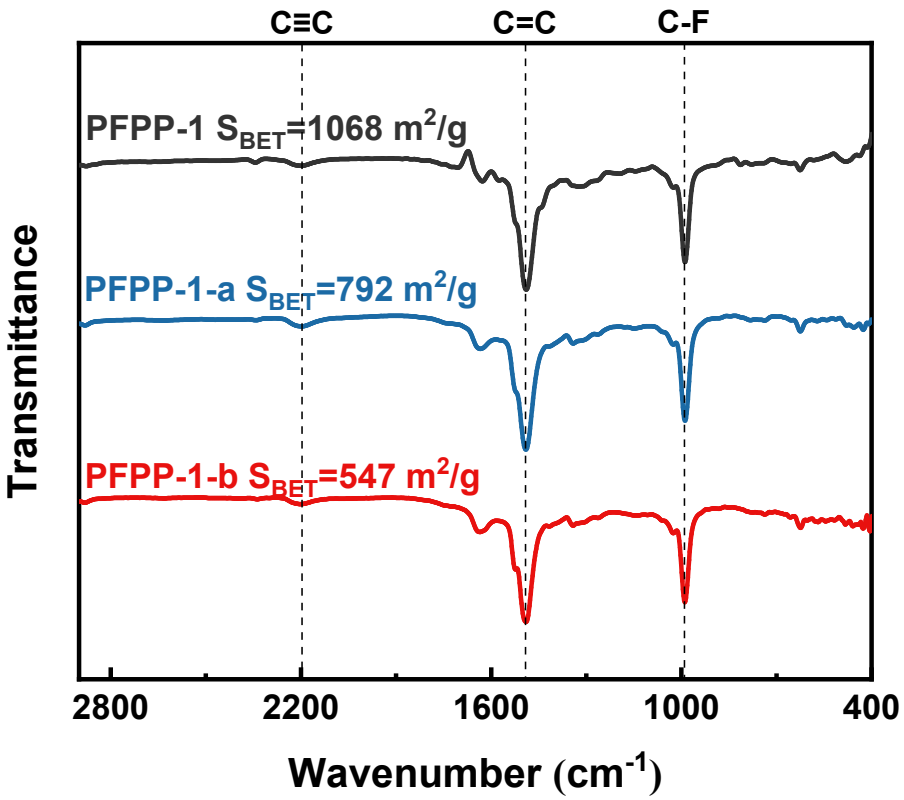

Fig. S7 The FT-IR spectra of the optimal PFPP-1, PFPP-1-a and PFPP-1-b synthesized under various conditions with various S_{BET}, shows that their primary chemical structures remain consitent. The enhancement in S_{BET} is solely achieved through optimization of reaction conditions.

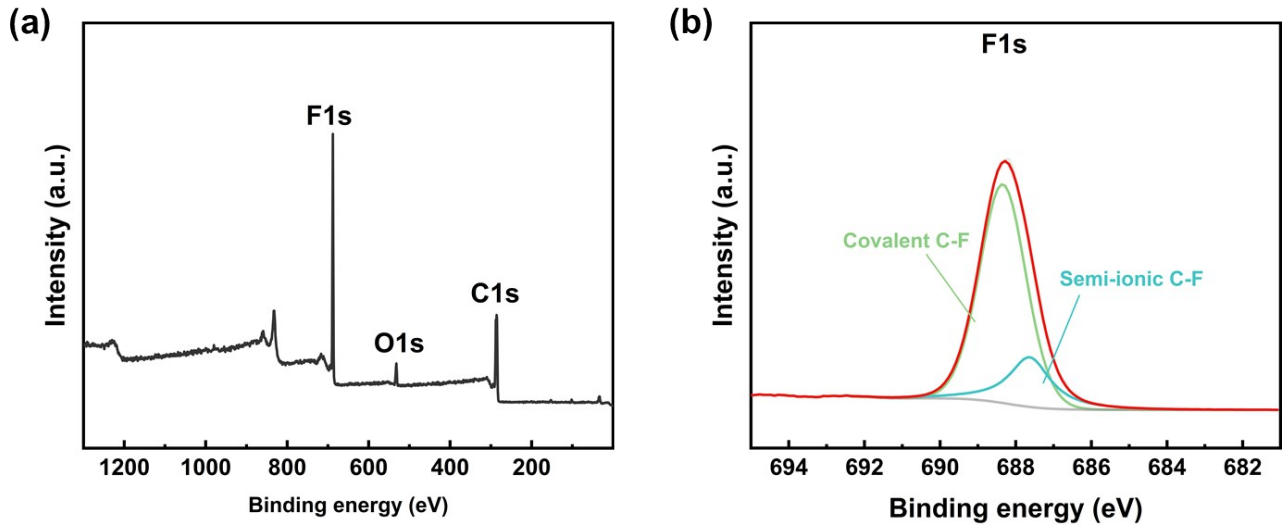

Fig. S8 (a) XPS wide-scan and (b) high-resolution C1s spectra of PFPP-1.

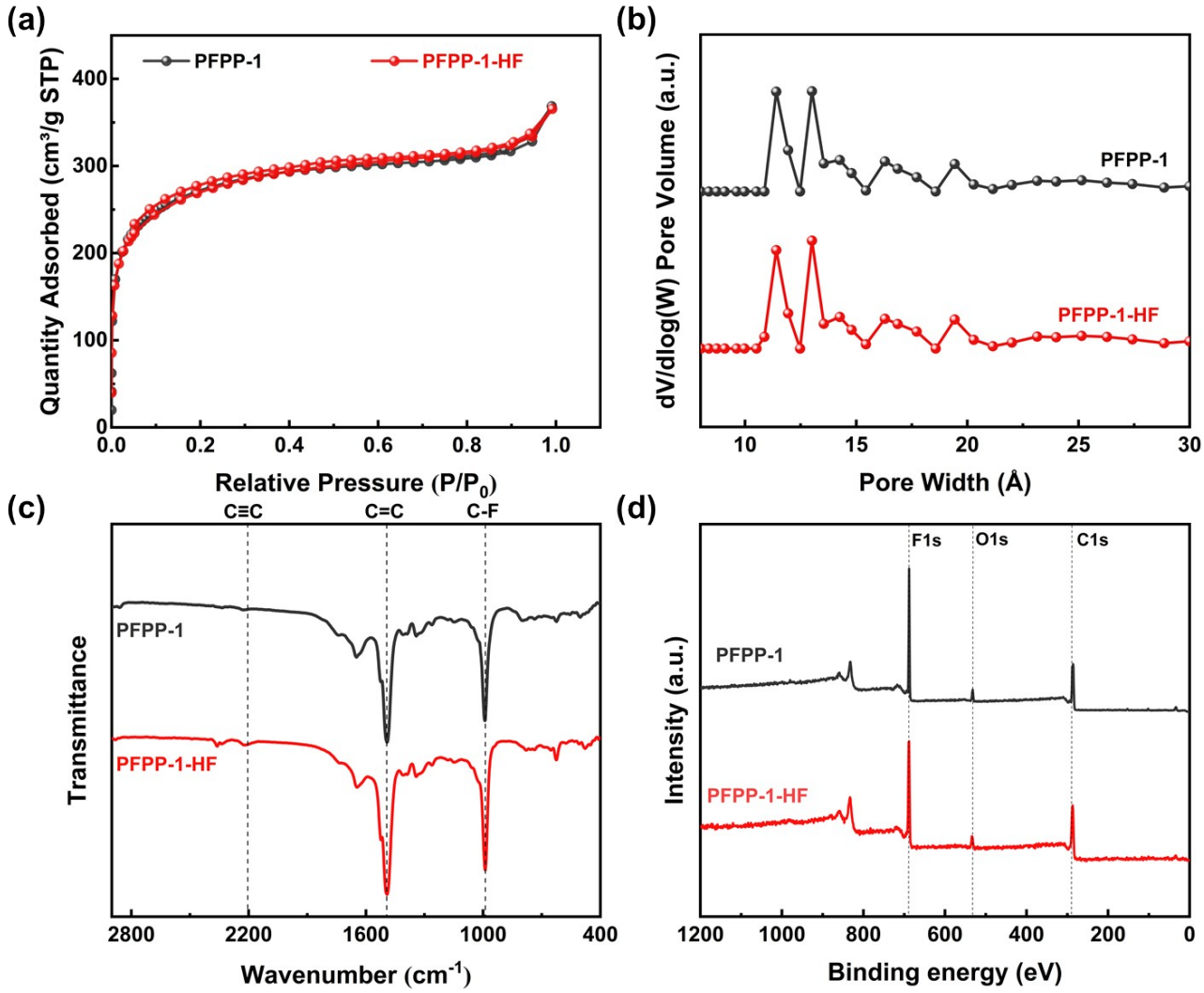

Fig. S9 Chemical and textural properties of PFPP-1. (a) N_2 isotherms at 77 K and (b) pore size distributions, (c) FT-IR spectra, (d) XPS wide-scan spectra of PFPP-1 before (black curves) and after (red curves) immersion in 40 wt.% HF solution for 7 days.

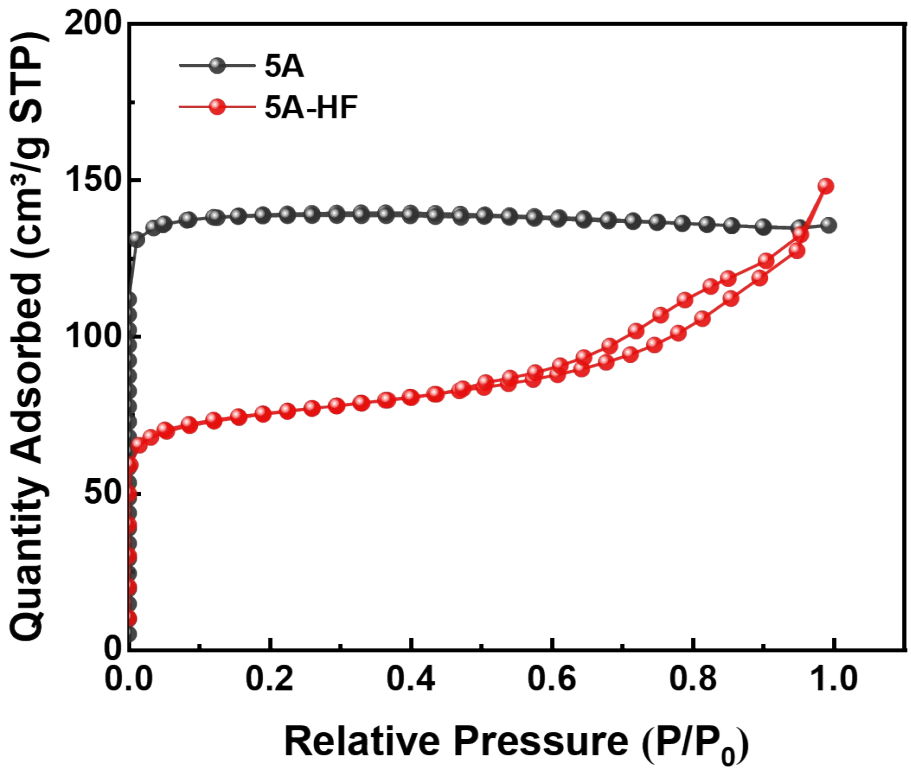

Fig. S10 N_2 adsorption-desorption isotherms at 77 K of pristine 5A zeolite and 5A zeolite immersed in 1wt.% HF solution for 2 hours. A significant change in the isotherms can be observed, with a decrease in porosity and the appearance of a hysteresis loop after brief exposure to HF.

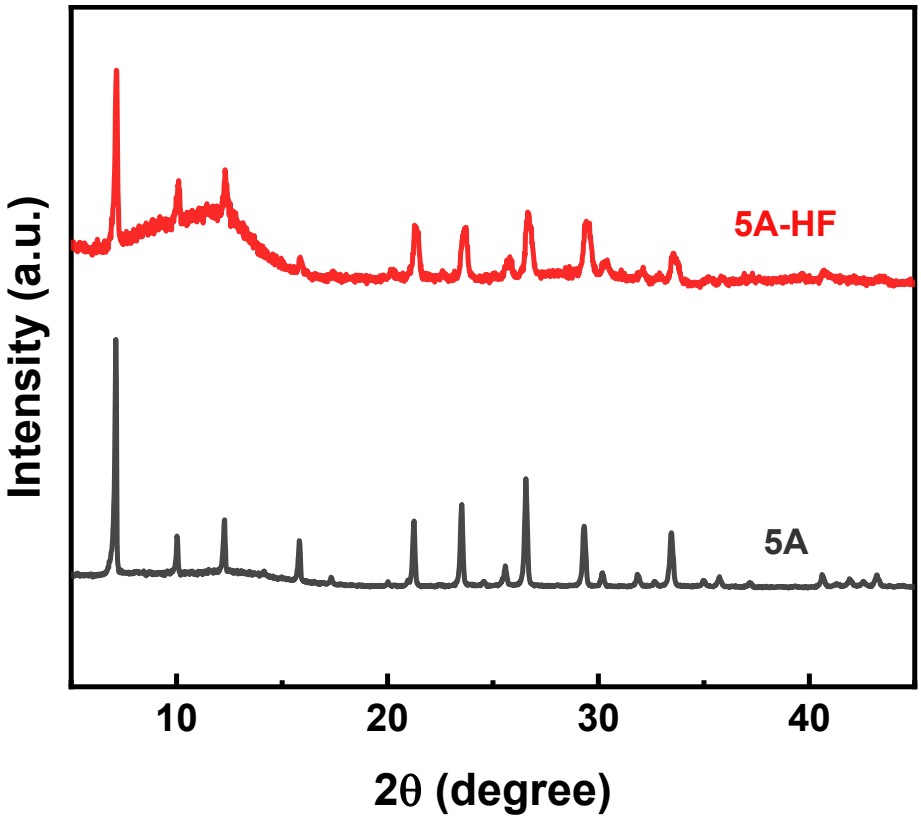

Fig. S11 PXRD patterns of pristine 5A zeolite and 5A zeolite immersed in 1wt.% HF solution for 2 hours. A significant change in the PXRD patterns can be observed, with a decrease in crystallinity and the appearance of amorphous regions after brief exposure to HF.

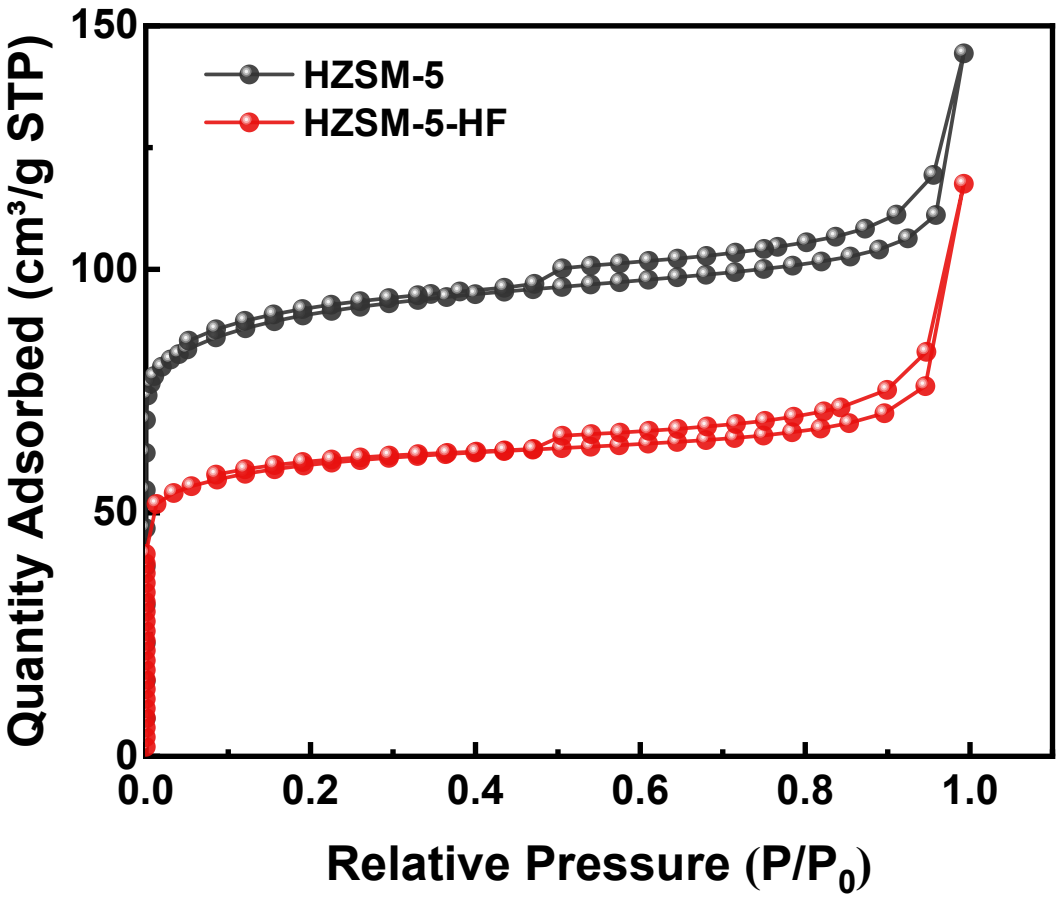

Fig. S12 N_2 adsorption-desorption isotherms at 77 K of pristine HZSM-5 zeolite and HZSM-5 zeolite immersed in 1wt.% HF solution for 2 hours. Although the isotherm shapes are similar, HZSM-5 experiences significant porosity loss after brief exposure to HF.

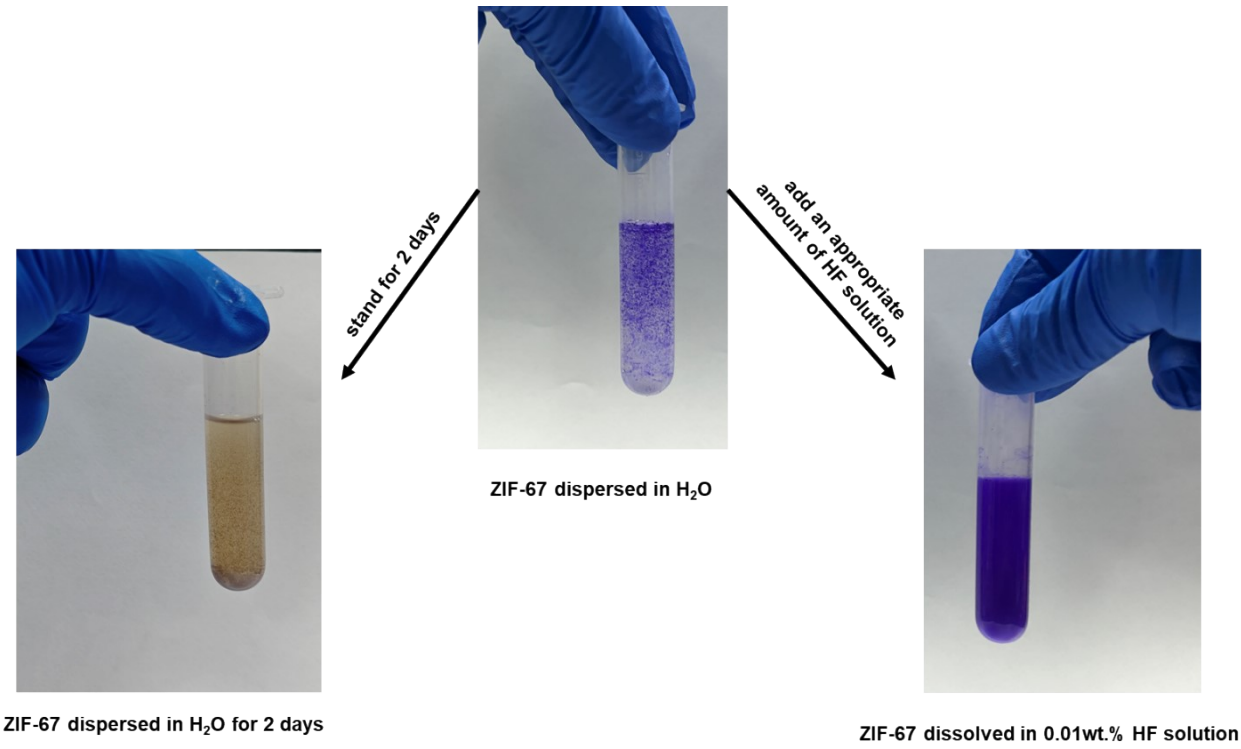

Fig. S13 Images of ZIF-67 dispersed in water, ZIF-67 after standing in water for 2 days, and ZIF-67 directly dissolved in weak acid. This demonstrates the weak stability of MOFs, even though ZIFs are considered relatively stable.

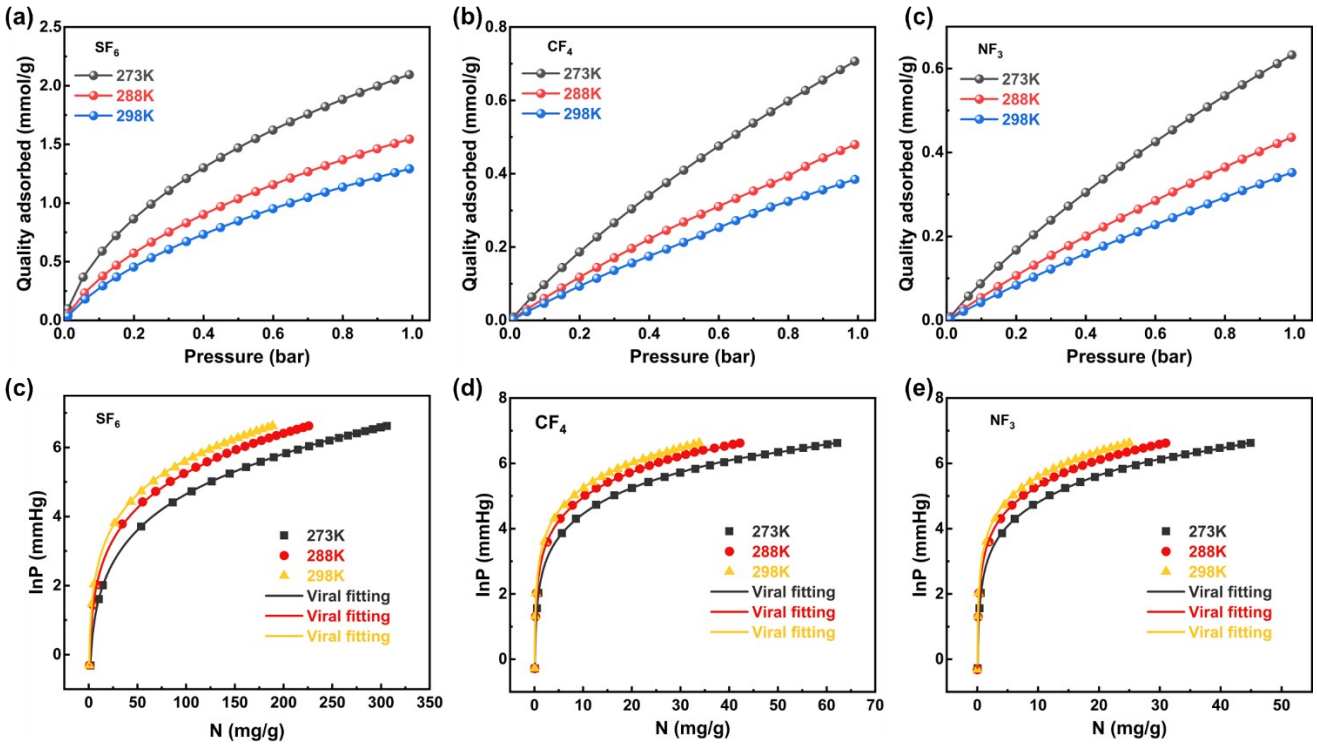

Fig. S14 Isotherms of SF_6 (a), CF_4 (b), and NF_3 (c) on PFPP-1 at 273 K, 288 K, and 298 K, respectively, along with the Virial fitting of the corresponding isotherms for SF_6 (d), CF_4 (e), and NF_3 (f).

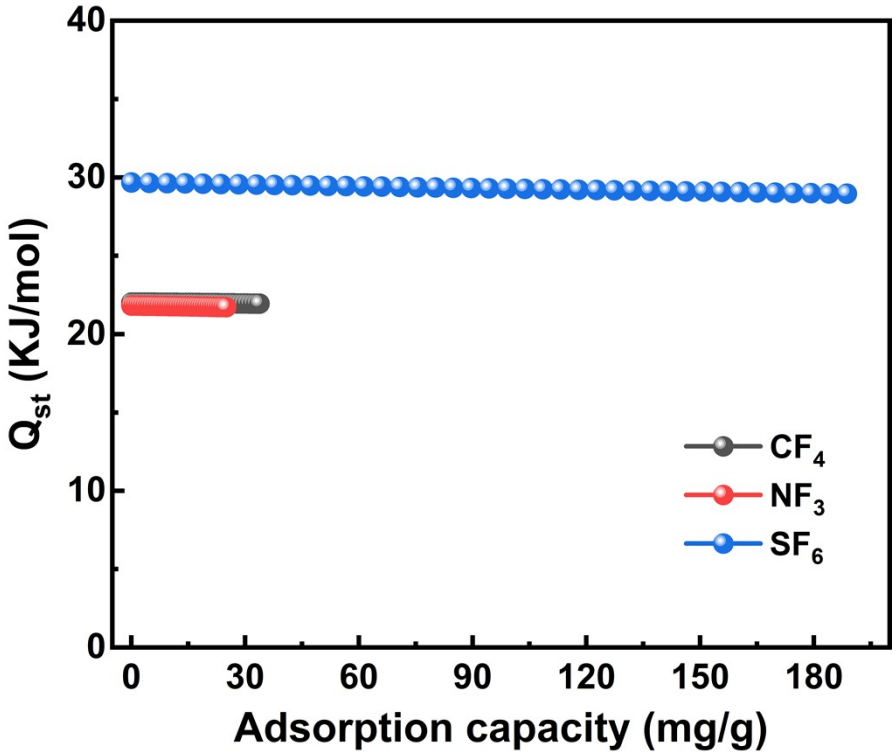

Fig. S15 The heat of adsorption (Q_{st}) of SF_6, CF_4, and NF_3 on PFPP-1 calculated by fitting the adsorption isotherms at varied temperatures using the Virial equation.

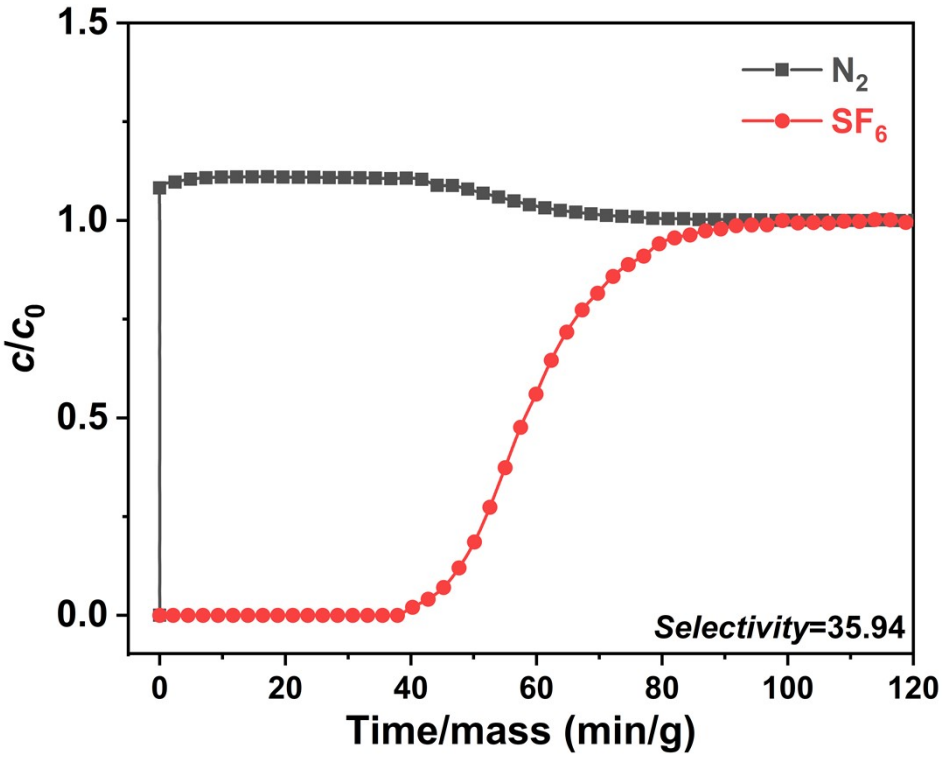

Fig. S16 Experimental breakthrough curves for the SF_6/N_2 mixture (1: 9) on PFPP-1 at 298 K and 1 bar, with a constant flow rate of 1.0 mL/min.

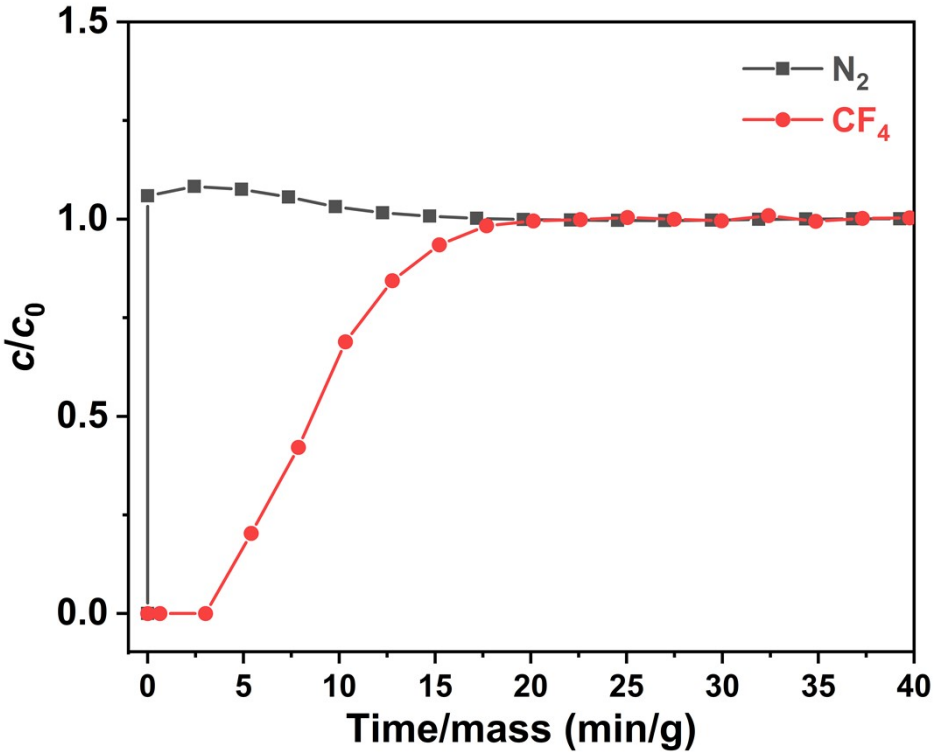

Fig. S17 Experimental breakthrough curves for the CF_4/N_2 mixture (1: 9) on PFPP-1 at 298 K and 1 bar, with a constant flow rate of 1.0 mL/min.

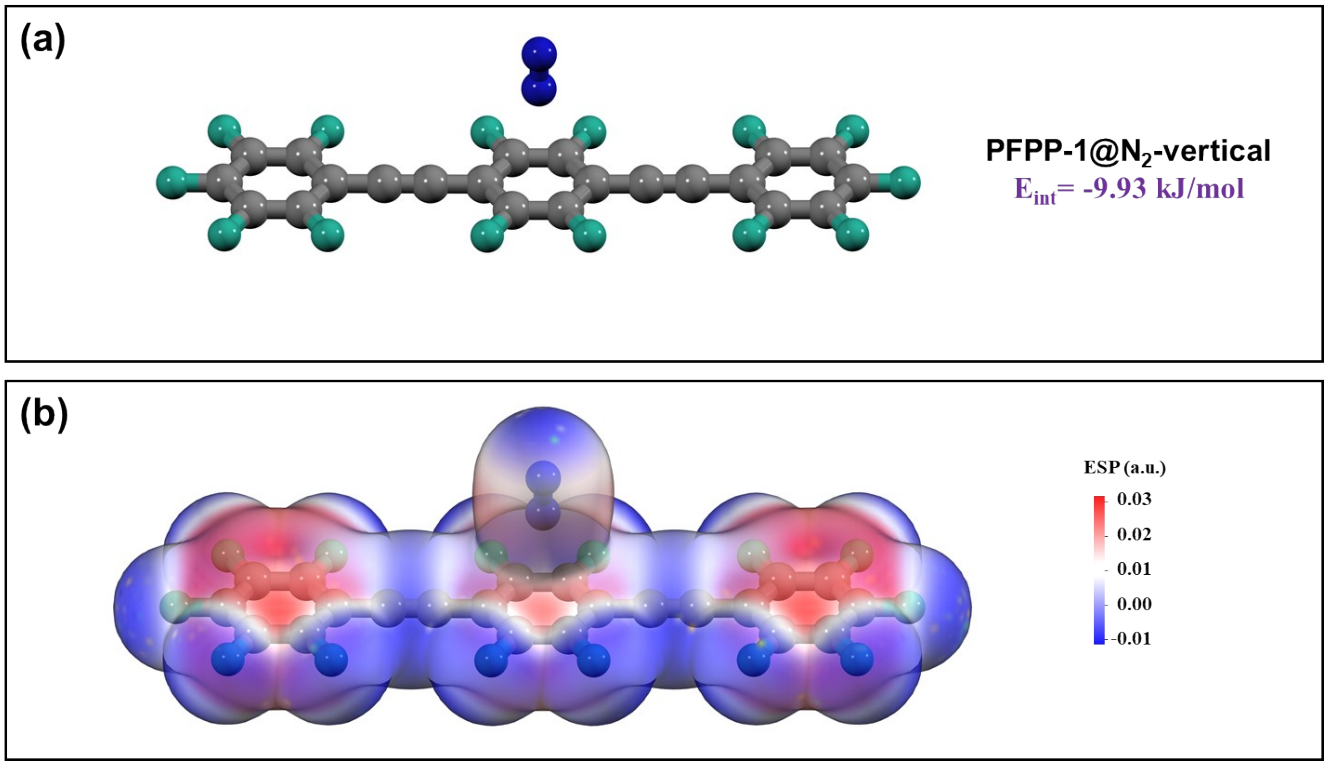

Fig. S18 (a) Simulated model and interaction energy (E_{Int}) of the binding structure between PFPP-1 and N_2 which adsorbs vertically above the benzene ring. (b) The electrostatic potential maps of corresponding structure.

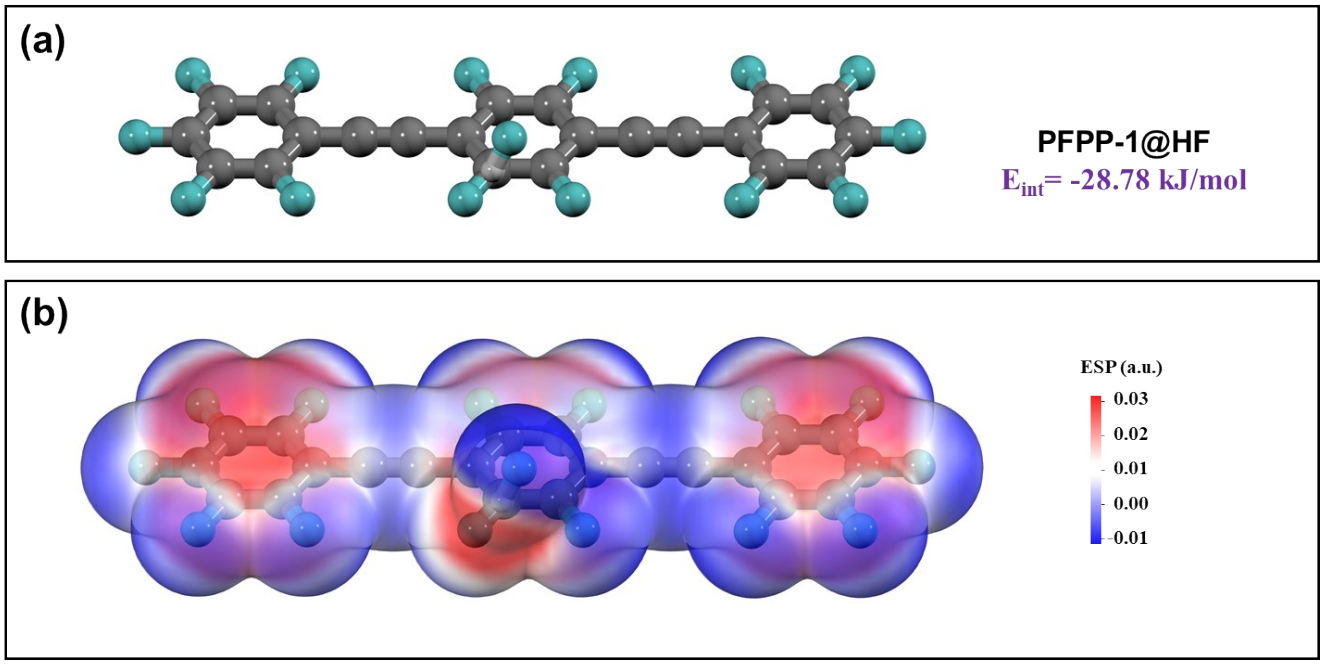

Fig. S19 (a) Simulated model and interaction energy (E_{Int}) of the binding structure between PFPP-1 and HF which adsorbs parallelly above the benzene ring. (b) The electrostatic potential maps of corresponding structure.

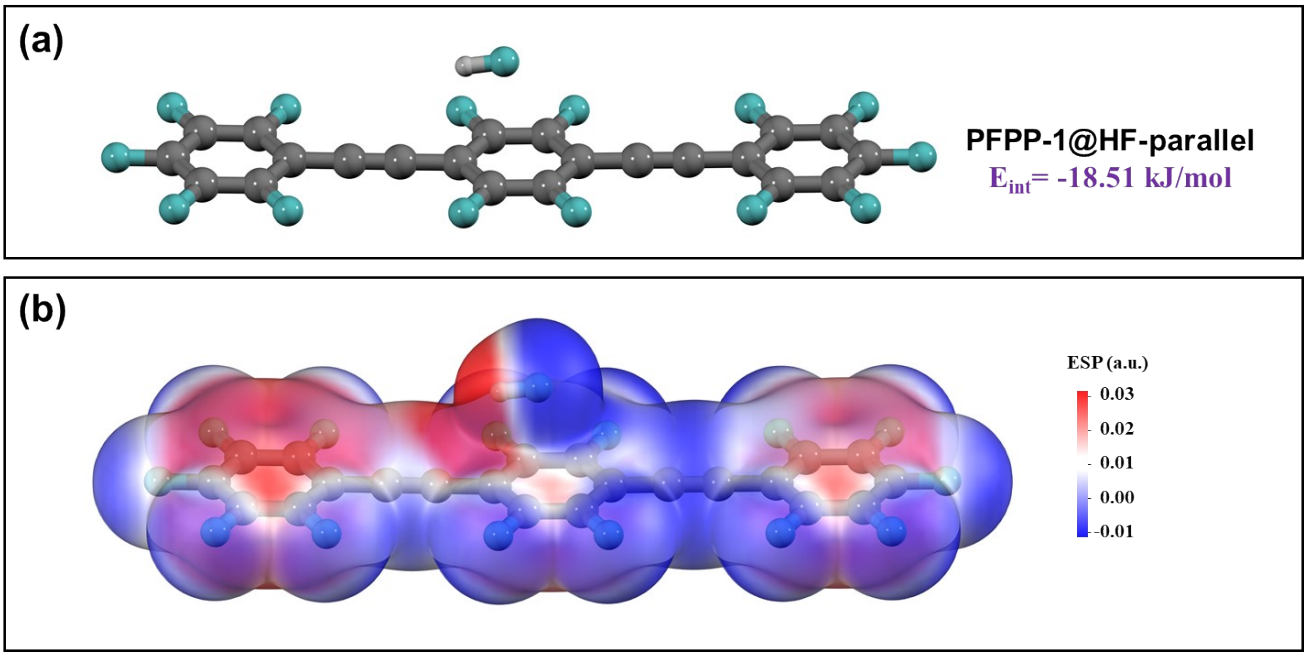

Fig. S20 (a) Simulated model and interaction energy (E_{Int}) of the binding structure between PFPP-1 and HF which adsorbs parallelly above the benzene ring. (b) The electrostatic potential maps of corresponding structure.

Table S1 Optimization for PFPP-1 synthesis

Sample	Monomer **A**	Monomer **B**	**B**/**A** ratio	Temperature (℃)	Catalysis	Catalysis amount[a] (mol%)	Catalysis droplet concentration (M)	Solvent	Yield[b] (%)	S_{BET} (m^2/g)
1[1]	PFB	TMSA	2	r.t.	TBAF	0.1	0.1	DMF	49	536
2	PFB	TMSA	2	25	TBAF	1	1	DMF	56.5	1068
3	OFN	TMSA	2	25	TBAF	1	1	DMF	11.0	459
4	OFN	BTMSA	2	25	TBAF	1	1	DMF	4.9	495
5	PFB	BTMSA	2	25	TBAF	1	1	DMF	33.8	513
6	PFB	TMSA	1	25	TBAF	1	1	DMF	41.4	768
7	PFB	TMSA	3	25	TBAF	1	1	DMF	62.9	1019
8	PFB	TMSA	2	10	TBAF	1	1	DMF	53.8	41
9	PFB	TMSA	2	35	TBAF	1	1	DMF	67.2	1079
10	PFB	TMSA	2	25	TMAF	1	1	DMF	39.2	342
11	PFB	TMSA	2	25	HF	1	1	DMF	-	-
12	PFB	TMSA	2	25	TBAF	0.1	1	DMF	3.1	479
13	PFB	TMSA	2	25	TBAF	0.5	1	DMF	18.3	1027
14	PFB	TMSA	2	25	TBAF	0.8	1	DMF	42.5	1072
15	PFB	TMSA	2	25	TBAF	1	0.1	DMF	76.9	379
16	PFB	TMSA	2	25	TBAF	1	0.5	DMF	62.3	549
17	PFB	TMSA	2	25	TBAF	1	1	THF	3.6	678
18	PFB	TMSA	2	25	TBAF	1	1	TL	13.1	546
19	PFB	TMSA	2	25	TBAF	1	1	MeOH	-	-

[a] Based on the molar amount of perfluoroarene; [b] Based on the mass of perfluoroarene.

Table S2 Comparison of S_{BET} and F content in various fluorinated porous polymers constructed via covalent bonds

Material	Category	Crystallinity	S_{BET} (m^2/g)	F content	Reference
PFPP-1	PFPPs	amorphous	1068	35.6 at.%[a] (45.7 wt.%)	This work
COP-177	COPs	amorphous	536	33.3 at.%[b]	[1]
COP-99	COPs	amorphous	479	14.3 at.%[a] (21.5 wt.%)	[17]
COP-175	COPs	amorphous	1035	13.1 at.%[b]	[18]
F-PDVB	HCPs	amorphous	771	22 at.%	[19]
POPTrB-8F	COPs	amorphous	628.9	33.62 at.%	[20]
POPTrA-8F	COPs	amorphous	507.1	22.95 at.%	[21]
F-CTF-1	CTFs	amorphous	662	17.0 at.%[a] (23.8 wt.%)	[22]
CTF-TF	CTFs	amorphous	407.7	22.6 at.%[a] (30.2 wt.%)	[23]
F-COF	COFs	crystalline	1275	34.97 wt.%	[24]
SCF-FCOF-1	COFs	crystalline	2056	13.30 wt.%	[25]
TF-COF 2	COFs	crystalline	2044	10.21 at.%	[26]

[a] Calculated from the mass fraction, if available. [b] Theoretical values were estimated based on the structure, as specific values were not provided in the original text.

Table S3 Comparison of C and F content of PFPP-1 from various elemental analysis methods

	XPS	EDS	EA	Theoretical value
C (at.%)	65.5	61.9	56.6 (45.9 wt.%)	66.7
F (at.%)	30.0	31.4	35.6 (45.7 wt.%)	33.3
C/F ratio	2.18	1.97	1.59	2

Table S4 Mass and S_{BET} changes of 5A and HZSM-5 before and after immersion in 1wt.% HF solution

	S_{BET} (m^2/g)	S_{BET} loss ratio (%)	Mass (g)	Mass loss ratio (%)
5A	478	-	0.5007	-
5A-HF	266	44	0.4679	6.55
HZSM-5	229	-	0.5528	-
HZSM-5-HF	187	18	0.4972	10.06

Table S5 Comparison of SF_6 adsorption capacities among various porous materials at 298 K and 1 bar.

Material	S_{BET} (m^2/g)	F content	Capacity (mmol/g)	Reference
PFPP-1	1068	35.6 at.%	1.21	This work
ANOP-8	694	14.86 at.%	0.92	[27]
POPTrA-4F	693.0	17.18 at.%	1.11	[21]
POPTrA-8F	507.1	22.95 at.%	1.03	[21]
Ppy-POF	641.9	-	0.84	[22]
UiO-66-Br_2	616	-	0.92	[28]
BrCOF-2-CF_3	1514	4.86 wt.%	1.45	[29]

Table S6 Physical parameters of selected gas adsorbates[20, 30-34]

Molecule	Dipole moment (10^{-18}·esu·cm)	Quadrupole moment (10^{-26}·esu·cm^2)	Polarizability (10^{-25}·cm^{-3})	Kinetic diameter (Å)
NF_3	0.235	-	36.2	4.5
CF_4	0	0	38.4	4.8
SF_6	0	0	65.4	5.2
HF	1.736	2.6	8.5	3.25*
N_2	0	1.52	17.4	3.64
O_2	0	0.39	15.8	3.46
H_2	0	0.662	8.0	2.89

* The kinetic diameter of single molecular HF, obtained through molecular simulation, falls between those of O_2 and H_2. The molecular model was constructed using GaussView and optimized at the PBE0/def2-TZVP level with Gaussian 16W to generate the wave function. The molecular kinetic diameter was estimated using Multiwfn software[35], based on the molecular electron density isosurface[32] at a value of 0.0015 a.u.

Table S7 Summary of the heat of adsorption (Q_{st}) of SF_6, CF_4, and NF_3 on PFPP-1 calculated by fitting the adsorption isotherms at varied temperatures using the Virial equation.

Structure	Q_{st} (kJ/mol)
SF_6	29.0
CF_4	22.0
NF_3	21.7

Table S8 Adsorption isotherm fitting parameters based on the Langmuir-Freundlich model.

Gas	Temperature	N_1	a	b	R^2
SF_6	298 K	2.26	1.27E-2	0.97	0.998
CF_4	298 K	1.57	9.53E-4	0.98	0.998
NF_3	298 K	1.48	9.11E-4	0.98	0.998
N_2	298 K	0.57	7.19E-4	1.14	0.997

Table S9 Summary of interaction energy (E_{Int})for various structures

Structure	E_{Int} (kJ/mol)
PFPP-1@N_2	-9.66
PFPP-1@N_2	-9.93
PFPP-1@SF_6	-24.65
PFPP-1@CF_4	-21.51
PFPP-1@NF_3	-21.60
PFPP-1@HF	-28.78
PFPP-1@HF-parallel	-18.51

Reference

1. S. Kim, D. Thirion, T. S. Nguyen, B. Kim, N. A. Dogan and C. T. Yavuz, *Chemistry of Materials*, 2019, **31**, 5206-5213.
2. C. Isanbor, *Journal of Physical Organic Chemistry*, 2017, **30**, e3687.
3. L. McDermott, D. C. Witkowski and N. K. Garg*, in *Organic Syntheses*, pp. 1-15.
4. S. Suzuki, M. R. Whittaker, E. Wentrup-Byrne, M. J. Monteiro and L. Grøndahl, *Langmuir*, 2008, **24**, 13075-13083.
5. P. J. Stephens, F. J. Devlin, C. F. Chabalowski and M. J. Frisch, *The Journal of Physical Chemistry*, 1994, **98**, 11623-11627.
6. S. Grimme, J. Antony, S. Ehrlich and H. Krieg, *The Journal of Chemical Physics*, 2010, **132**.
7. P. C. Hariharan and J. A. Pople, *Theoretica chimica acta*, 1973, **28**, 213-222.
8. W. J. Hehre, R. Ditchfield and J. A. Pople, *The Journal of Chemical Physics*, 1972, **56**, 2257-2261.
9. Y. Zhao and D. G. Truhlar, *Theoretical Chemistry Accounts*, 2008, **120**, 215-241.
10. R. Krishnan, J. S. Binkley, R. Seeger and J. A. Pople, *The Journal of Chemical Physics*, 1980, **72**, 650-654.
11. T. Dutta, K. B. Woody and M. D. Watson, *Journal of the American Chemical Society*, 2008, **130**, 452-453.
12. K. O. Christe, W. W. Wilson, R. D. Wilson, R. Bau and J. A. Feng, *Journal of the American Chemical Society*, 1990, **112**, 7619-7625.
13. H. Sun and S. G. DiMagno, *Journal of the American Chemical Society*, 2005, **127**, 2050-2051.
14. R. K. Sharma and J. L. Fry, *The Journal of Organic Chemistry*, 1983, **48**, 2112-2114.
15. R. Dawson, A. Laybourn, Y. Z. Khimyak, D. J. Adams and A. I. Cooper, *Macromolecules*, 2010, **43**, 8524-8530.
16. J. Chen, W. Yan, E. J. Townsend, J. Feng, L. Pan, V. Del Angel Hernandez and C. F. J. Faul, *Angewandte Chemie International Edition*, 2019, **58**, 11715-11719.
17. J. Byun, H. A. Patel, D. Thirion and C. T. Yavuz, *Nature Communications*, 2016, **7**, 13377.
18. D. Thirion, Y. Kwon, V. Rozyyev, J. Byun and C. T. Yavuz, *Chemistry of Materials*, 2016, **28**, 5592-5595.
19. Y. Luo, Z. Yang, X. Suo, H. Chen, T. Wang, Z. Wang, Y. Liu, Y. Lyu, I. Popovs and S. Dai, *Nano Research*, 2021, **14**, 3282-3287.
20. W. Zhang, Y. Wu, Y. Li, S. Chen, Y. Fu, Z. Zhang, T. Yan, S. Wang and H. Ma, *Macromolecules*, 2022, **55**, 1435-1444.
21. W. Zhang, Y. Li, Y. Wu, Y. Fu, S. Chen, Z. Zhang, S. He, T. Yan and H. Ma, *Separation and Purification Technology*, 2022, **287**, 120561.
22. Y. Zhao, K. X. Yao, B. Teng, T. Zhang and Y. Han, *Energy & Environmental Science*, 2013, **6**, 3684-3692.
23. L. Guan, Z. Guo, Q. Zhou, J. Zhang, C. Cheng, S. Wang, X. Zhu, S. Dai and S. Jin, *Nature Communications*, 2023, **14**, 8114.
24. W. A. Braunecker, K. E. Hurst, K. G. Ray, Z. R. Owczarczyk, M. B. Martinez, N. Leick, A. Keuhlen, A. Sellinger and J. C. Johnson, *Crystal Growth & Design*, 2018, **18**, 4160-4166.
25. Q. Liao, C. Ke, X. Huang, G. Zhang, Q. Zhang, Z. Zhang, Y. Zhang, Y. Liu, F. Ning and K. Xi, *Journal of Materials Chemistry A*, 2019, **7**, 18959-18970.
26. S. B. Alahakoon, G. T. McCandless, A. A. K. Karunathilake, C. M. Thompson and R. A. Smaldone, *Chemistry – A European Journal*, 2017, **23**, 4255-4259.

27. J. Zhu, D. Luo, Q. Wang, S. Tong, Z. Wang and J. Yan, *Chemical Communications*, 2024, **60**, 12209-12212.
28. M.-B. Kim, K.-M. Kim, T.-H. Kim, T.-U. Yoon, E.-J. Kim, J.-H. Kim and Y.-S. Bae, *Chemical Engineering Journal*, 2018, **339**, 223-229.
29. Q. Liao, C. Ke, X. Huang, D. Wang, Q. Han, Y. Zhang, Y. Zhang and K. Xi, *Angewandte Chemie International Edition*, 2021, **60**, 1411-1416.
30. J.-R. Li, R. J. Kuppler and H.-C. Zhou, *Chemical Society Reviews*, 2009, **38**, 1477-1504.
31. S. Sircar, *Industrial & Engineering Chemistry Research*, 2006, **45**, 5435-5448.
32. N. Mehio, S. Dai and D.-E. Jiang, *The Journal of Physical Chemistry A*, 2014, **118**, 1150-1154.
33. D. Spelsberg and W. Meyer, *The Journal of Chemical Physics*, 1994, **101**, 1282-1288.
34. K. M. Gough, M. M. Yacowar, R. H. Cleve and J. R. Dwyer, *Canadian Journal of Chemistry*, 1996, **74**, 1139-1144.
35. T. Lu and F. Chen, *Journal of Computational Chemistry*, 2012, **33**, 580-592.